Electron probe microanalysis of light elements: Improvements in the measurement and signal extraction methods

Pia Schweizer, Emmanuelle Brackx, Philippe Jonnard

Received: 29 January 2022 | Revised: 30 March 2022 | Accepted: 26 April 2022

DOI: 10.1002/xrs.3290

RESEARCH ARTICLE

X-RAY SPECTROMETRY WILEY

Electron probe microanalysis of light elements: Improvements in the measurement and signal extraction methods

Pia Schweizer[1] | **Emmanuelle Brackx**[1] | **Philippe Jonnard**[2]

[1]CEA, DES, ISEC, DMRC, Universite Montpellier, Marcoule, France

[2]Faculté des Sciences et Ingénierie, UMR CNRS, Laboratoire de Chimie Physique - Matière et Rayonnement, Sorbonne Université, Paris Cedex, France

Correspondence
Pia Schweizer, CEA, DES, ISEC, DMRC, Universite Montpellier, Marcoule, France.
Email: pia.schweizer@cea.fr

Funding information
CEA cross-cutting basic research Programme RBNEW

Abstract

Quantitative electron probe microanalysis (EPMA) by wavelength dispersive spectrometry of light elements is a significant challenge due to difficulties of signal extraction for low intensities. Therefore, a good choice of measurement parameters and a suitable signal treatment, accurate background description and interference correction are crucial. For light elements, peak to background ratios (P/B) can easily approach unity and special care needs to be paid to the setting of the pulse height analyser (PHA) to avoid noise contribution to the emission peak. Furthermore, the background may have a high curvature and the classical approach of a linear background fit is no longer valid. This work investigates the EPMA of light elements from Be to F with the aim to determine the best experimentation parameters (dispersive element, accelerating voltage, PHA). It also provides detailed information about peak shifts, peak broadening and the influence of different background fits on quantification. In total, 25 samples containing light elements were analysed and Monte Carlo simulations were carried out. These simulations show that the X-ray intensity of the light element's characteristic line can be increased by working with low accelerating voltages around 5 kV. PHA should be used in automatic differential or integral mode. Our work also shows that a third degree linear polynomial describes the background better than an exponential or linear function. Consequently overestimation of P/B values leading to large quantification errors can be avoided. This paper provides a large database containing peak position and peak shifts, peak full width at half maximum, as well as P/B ratios and information about peak enlargement for different materials of various compositions.

KEYWORDS

area/peak factors, background subtraction, electron probe microanalysis, light elements, micoanalyser parameters

1 | INTRODUCTION

Electron probe microanalysis (EPMA), a non-destructive technique using wavelength dispersive X-ray spectrometry (WDS), nowadays allows to quantitatively analyse most of inorganic samples. Nevertheless, quantification of samples containing light elements from lithium to fluorine is still complicated due to the difficulties of signal extraction. The presence of light elements in a large variety of materials, for example energy storage materials, high temperature materials with resistant coatings or even tailored ceramics, leads to an increasing interest in characterising these substances at a micron scale to better understand and improve their properties.

After the pioneer work of Castaing, Bastin et al. focussed for the first time on the problems of EPMA of light elements in the late 1980s[1,2] and there has been great progress, especially in instrumentation and signal processing. The implementation of recently developed periodic multilayers in today's microanalysers allows spectroscopy of light elements,[3] even at extreme low energies in the Li K range.[4] Even though quantitative EPMA of light elements is possible in theory, there are many difficulties to overcome.

Light elements have a much lower fluorescence yield than heavy elements, which leads to less emission of X-rays in favour of Auger electrons. Due to their low energy, the few X-rays emitted are easily absorbed by the sample or by detector windows. In the end, net intensity of characteristic X-ray peaks of light elements is that low that accurate determination and subtraction of the background is crucial. When peak/background (P/B) ratios approach unity, even small imprecisions in background description can lead to considerable errors in quantification.[5] The common approach of a linear regression between two points chosen at the low and high energy sides of the peak is no longer acceptable[6] and background curvature has to be taken into account.

Furthermore, the spectral distance between X-ray lines decreases with their energy and spectral interference between the emission lines of light elements and the L, M, or N lines of heavy elements is a frequent phenomenon (e.g. B Kα and Mo Mζ or Li Kα and Mg L and Al L).[7] To counter intensity measurement errors caused by the superposition of other emission lines and higher diffraction orders, special attention needs to be payed to the detection window setting of the pulse height analyser connected to the proportional counter during the measurement process and to the data treatment later on. Knowledge about the expected peak positions before an analysis helps to determine if a separation of different emission lines will be possible. The peak position of Kα lines of light elements, though, are subjected to matrix effects, that is, the changes in chemical bonding as a function of different material compositions. These effects also lead to peak shape changes.

This work investigates the WDS EPMA of light elements from Be to F. Its aim is to determine the best experimental parameters and to give detailed information about peak position, peak broadening and influence of background subtraction on P/B values.

2 | METHODS AND MATERIALS

2.1 | Mathematical concepts

We first briefly review the mathematical concepts important for the signal treatment of the experimental data. The natural shape of characteristic X-ray lines produced by transitions between two core levels is the convolution of the two core levels density of states (DOS). Both DOS are Lorentzians

$$L(E) = \frac{H}{1 + \left(\frac{E - E_0}{\gamma/2}\right)^2}, \tag{1}$$

where γ is the full width at half maximum (FWHM) of the line, H its amplitude and E_0 its central energy (known as characteristic energy). Thus, the resulting shape of an atomic line is Lorentzian and its width is equal to those of the core levels.

Equation (1) is nevertheless not exact for the Kα emission of light elements, as the transition involves valence electrons.[8] The shape of a light element's emission band is the convolution of Equation (1) and the DOS in the valence band, which is around 5 eV to 10 eV wide for light elements.

The response function of the spectrometer has a Gaussian shape

$$F(E) = H\exp\left[-\ln 2 \cdot \left(\frac{E - E_0}{\Gamma/2}\right)^2\right], \tag{2}$$

where Γ is its FWHM.

The actual form of the detected X-ray emission bands is a convolution of these distributions, even if it can be governed by the Gaussian contribution. Figure 1a shows the calculated local and partial DOS of SiO_2 stishovite and in (b) the calculated O Kα emission band, that corresponds to the transition O 2p-1s, the calculated reflectivity curve of the W/Si multilayer, and the simulated spectrum compared to the experimental one. As one can see on Figure 1a, the top of the valence band is

dominated by the O 2p states with a total bandwidth of about 10 eV the FWHM being approximately 4 eV. To calculate the O Kα transition, the local and partial O 2p DOS is weighted by the elements of the transition matrix and convolved with a Lorentzian of 0.15 eV width,[9] representing the O 1s core level, with a Lorentzian of variable width representing the hole in the valence band (max. 1 eV) and with a Gaussian representing the experimental broadening. For a suitable comparison to our experiment, the width of the Gaussian contribution is set to 10 eV, as this corresponds to the width of the calculated reflectivity curve. The width difference between the reflectivity curve and the measured emission line is mainly due to the contribution of the valence band, but there may be other experimental factors that slightly enlarge the measured line. The asymmetry of the measured peak is caused by the increasing background intensity for higher photon energies.

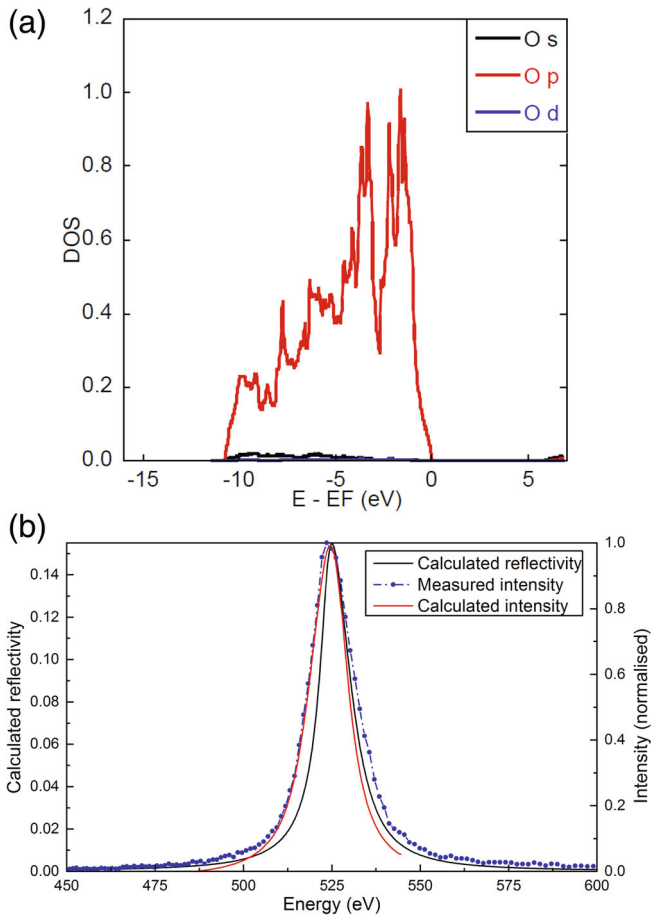

FIGURE 1 (a) Local and partial O DOS of SiO_2 stishovite. EF corresponds to the Fermi level. (b) Calculated reflectivity curve of a W/Si multilayer (see Table 1), calculated O Kα emission of a SiO_2 sample (the width of the Gaussian contribution was set to 10 eV) and observed emission at 12 kV acceleration voltage. [Colour figure can be viewed at wileyonlinelibrary.com]

The detected peak form can be written as the convolution of Equation (2) with a convolution of Equation (1) and the DOS in the light element's valence band.

Provided the DOS width is small with respect to the experimental broadening, the resulting function has a Voigt profile. An easier to use, valid approximation[10] to describe the peak shape in EPMA is the linear expression

$$P(E) = H\left[(1-k)\exp\left(-\ln 2\cdot\left(\frac{E-E_0}{\Gamma/2}\right)^2\right) + \frac{k}{1+\left(\frac{E-E_0}{\Gamma/2}\right)^2}\right] \quad (3)$$

called Pseudo-Voigt function, where Γ corresponds to the FWHM dominated by the Gaussian contribution. k is the weight factor for Gaussian and Lorentzian distribution and varies from $k=1$ (pure Lorentzian) to $k=0$ (pure Gaussian).

Depending on the chemical state of the light element, the shape of the emission peak is exposed to strong alterations, the maximal intensity value is no longer representative of its integral intensity and it is necessary to carry out the measurement over the whole spectral width of the peak. Fitting the experimental data with Equation (3) allows determining this integral intensity. Nevertheless, the measurement process can be impactfully long, especially when several measurement series in similar conditions have to be carried out.

2.1.1 | Area/peak factor

Proposed by Bastin et al.,[1] the introduction of area/peak factors (APFs) is a timesaving concept. This factor can be understood as follows: there is a fixed proportion between the k-ratio calculated with the integral intensity

TABLE 1 Wavelength dispersive X-ray spectrometry multilayers for light element analysis in a domain for Bragg angles between 13° and 55°

Crystal	2d (nm)	Analysis domain		Detectable X-rays		
		λ (nm)	Energy (keV)	K	L	M
W/Si	6.0	1.35–4.91	0.92–0.25	C to Ne	K to Cu	La to Pr
Ni/C	9.5	2.14–7.78	0.58–0.16	B to O	Cl to Cr	Nb to Ag
Mo/B_4C	20.0	4.50–16.38	0.28–0.08	Be to C	Al to K	Rb to Pd

(area) of the peak and the standard k-ratio, calculated with the maximum intensity. This APF factor can be calculated for a given standard and spectrometer and can be used in further measurements as a weighting parameter for the peak intensity relative to the integral intensity of a standard. At this point, it is important to mention that two chemical states of one element do not necessarily lead to the same shape of the emission band. The use of APFs in our case can be justified by the fact that the Gaussian contribution of the spectrometer prevails, see also Figure 1. The advantage of calculating these factors is that other measurements in similar conditions can simply be carried out on the peak. The APFs should not be confused with the FWHM, which is often insensitive to peak shape alterations.

For calculating these factors, it is, though, necessary to perform an accurate background subtraction.

2.1.2 | Background description

For high P/B-values, the background values are in most cases taken at the left and the right edges of the peak and assumed to vary linearly between these two points, which is generally a suitable hypothesis. Contrary to this, for the quantitative EPMA of light elements, background curvature has to be taken into account. As there may be, in addition, interferences and absorption edges that influence the peak shape and the background, these phenomena should be considered in the background subtraction.[6]

However, it is almost impossible to construct an exact analytical model based on a physical description of the problem. A flexible and therefore commonly used method consists in least-squares fitting of the acquired data with an analytical function.[11] As there are many physical processes contributing to the background, it may be useful to describe it as some type of polynomial function.

Linear polynomial

A function of the type

$$y_B(i) = a_0 + a_1(E_i - E_0) + a_2(E_i - E_0)^2 + \ldots \\ \ldots + a_k(E_i - E_0)^k \quad (4)$$

can describe the background on a small interval. E_i is the energy of the channel i and E_0 is some reference energy. The degree of the polynomial $k = 0$, 1 and 2 leads to a constant, linear or a parabolic description of the background, respectively. Polynomials with $k \geq 3$ should be used carefully as higher orders can lead to non-realistic oscillations.

Exponential polynomial

If the background continuum shows a strong curvature, or if a complete description over a large spectrum region is required, using an exponential polynomial of the type

$$y_B(i) = a_0 \exp\left[a_1(E_i - E_0) + a_2(E_i - E_0)^2 + \ldots \right. \\ \left. \ldots + a_k(E_i - E_0)^k\right] \quad (5)$$

can be appropriate. Due to the non-linearity of the parameters a_1, ..., a_k which have to be estimated beforehand, the fitting procedure is more complicated. Since the energy range of WDS crystals used for EPMA of light elements is only a few hundred eV, the expression (5) can be simplified using $k = 1$ and is still suitable to describe the spectrum with high curvature.

2.2 | Simulation software

First, the usage of simulation tools can help to determine the best measurement parameters. Second, simulated emission spectra can be used as standard for quantitative analysis.

Monte Carlo (MC) simulations based on reliable electron interaction models and large numerical databases have proven their benefits for EPMA.[12] The program PENEPMA, using the general-purpose code system PENELOPE, performs MC simulations of coupled electron photon transport for complex material structures and covers the energy range from 1 GeV down to 50 eV[13] even if the cross section and absorption coefficient data under 1 keV can have uncertainties up to 200%. Hence, the results of simulations for samples containing light elements have to be taken with caution. The X-ray energies of K-shell transitions of light elements are taken from Reference 14. For an exact description of all interaction databases used in PENEPMA, please see Reference 15.

Another program using MC simulations is CASINO,[16] particularly adapted for quick signal predictions for low-energy beam interaction in electron microscopy of a bulk or thin foil. This easy to use program helps planning the analysis.

In this work, CASINO simulations were used to predict the X-ray intensity as a function of the accelerating voltage to determine the value at which X-ray emission of the light element is maximum but for which heavier elements are still excited. Some of the results are shown in Figure 2. As one can see, characteristic intensity of light elements is highest for low accelerating voltages. If analyses are carried out on samples containing light and heavy elements (e.g. Figure 2b,c), a compromise has to be

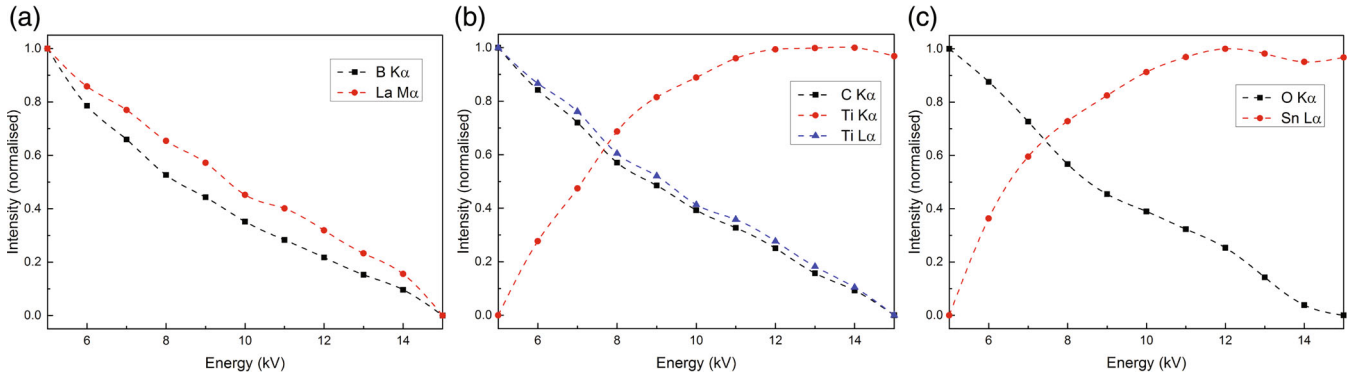

FIGURE 2 Normalised intensity of the characteristic X-rays as a function of the accelerating voltage applied to the microanalyser for the materials (a) LaB_6, (b) TiC and (c) SnO_2. The characteristic intensity depends on the ionisation cross section, the material's fluorescence yield and its absorption coefficient. Several Monte Carlo simulations are performed for every point and the statistical uncertainties are negligible compared to the large uncertainties in the database values used in the simulation software. [Colour figure can be viewed at wileyonlinelibrary.com]

found to guarantee excitation of the heavy elements. In that case, accelerating voltages between 5 and 9 kV may be the best choice.

The spectra obtained by PENEPMA simulations were superposed later on to the measured spectra. This helps visualising peak-shifts and identifying satellite and multiple-order diffraction peaks present on the measured spectra.

2.3 | Multilayers and analysed materials

Measurements were carried out on a CAMECA microprobe SXFive FE TACTIS that has five spectrometers with up to four dispersive elements. The diameter of the Rowland circle is 320 mm, large enough that there are no further collimating slits required to obtain a good spectral resolution. Since the wavelength of characteristic photons emitted by light elements is long, they cannot be diffracted by natural crystals, but only by multilayer structures consisting of periodically alternating thin bilayers of heavy and light elements with large periods. Table 1 lists the different multilayers that were used for our purpose, the CAMECA manufacturer's data on multilayer periods and the resulting analysis domain.

We focused in this work on the qualitative EPMA of different materials containing light elements from Be to F listed below. The analysed bulk samples are pure chemical compounds with some nm of carbon coating to avoid charge-up effects. For each light element's mass fraction in the samples, see Table 2.

- beryllium (Be) [Mo/B_4C multilayer]
- boron (B), lanthanum hexaboride (LaB_6), boracite, ($Mg_3B_7O_{13}Cl$), danburite ($CaB_2(SiO_4)_2$), molybdenum (Mo) [multilayer Mo/B_4C]
- carbon (C), silicon carbide (SiC), titanium carbide (TiC) [Ni/C and W/Si multilayers]
- silicon nitride (Si_3N_4), gallium nitride (GaN), tantalum nitride (TaN) [Ni/C and W/Si multilayers]
- silicon dioxide (SiO_2), wollastonite ($CaSiO_3$), magnesium oxide (MgO), fluorapatite ($Ca_5(PO_4)_3F$), andradite ($Ca_3Fe_2(SiO_4)_3$), zircon ($ZrSiO_4$), barium sulphite ($BaSO_4$), manganese oxide (MnO), tin dioxide (SnO_2), cerium dioxide (CeO_2) [Ni/C and W/Si multilayers]
- cerium trifluoride (CeF_3), praseidymium trifluoride (PrF_3), neodymium trifluoride (NdF_3) [Ni/C (second diffraction order at $E_{peak}/2$) and W/Si multilayers]

The photons diffracted by the multilayers are counted in a proportional counter filled with a mixture of argon/methane gas.

3 | EXPERIMENTAL DATA ACQUISITION AND ANALYSIS PROCEDURE

3.1 | Settings

The different measurements were carried out at an acceleration voltage of 12 kV and an electron beam current of 10 nA. Even if lower acceleration voltages between 5 and 10 kV can lead to higher emission of characteristic X-rays of light elements,[17] we decided to not change the parameter in a first time to ensure the continuity of other measurements carried out in the same period. For each sample, the characteristic spectrum is acquired over the entire range of the analysing multilayer(s) that is divided into 600 steps. This determines the number of steps acquired around the peak. 600 steps over the whole energy spectrum are enough to not penalise the spectral

TABLE 2 Light element's mass fraction in the material, peak centre of the Kα emission line, peak shift (simulated positions of the Kα emission lines: Be 108.5 eV, B 183.3 eV, C 277.0 eV, N 392.4 eV, O 524.9 eV, F 676.8 eV) and line full width at half maximum (FWHM)

Emission	Material	Mass fraction	E_{peak} (eV)	Peak shift (eV)	FWHM (eV)
Be Kα	Be	1	104.3	4.2	6.4
	B	1	183.2	0.1	14.7
	LaB_6	0.32	183.3	0	13.6
B Kα	$Mg_3B_7O_{13}Cl$	0.19	181.4	1.9	14.1
	$CaB_2(SiO_4)_2$	0.09	181.2	2.1	13.5
Mo Mζ	Mo	0	194.2	1.2	27.2
	C	1	278.0	1.0	14.9
C Kα	SiC	0.30	277.2	0.2	12.4
	TiC	0.20	278.7	1.7	10.9
	Si_3N_4	0.40	393.0	0.6	10.8
N Kα	GaN	0.17	393.5	1.1	9.3
	TaN	0.07	392.9	0.5	6.6
	SiO_2	0.52	524.9	0	15.1
	$CaSiO_3$	0.41	525.1	0.2	14.7
	MgO	0.40	525.5	0.6	14.7
	$Ca_5(PO_4)_3F$	0.38	525.1	0.2	15.5
O Kα	$Ca_3Fe_2(SiO_4)_3$	0.38	525.5	0.6	14.8
	$ZrSiO_4$	0.35	525.5	0.6	15.1
	$BaSO_4$	0.27	525.3	0.4	14.9
	MnO	0.23	525.1	0.2	14.6
	SnO_2	0.21	525.1	0.2	14.6
	CeO_2	0.19	525.1	0.2	14.6
	CeF_3	0.29	676.8	0	24.8
F Kα	PrF_3	0.29	677.5	0.7	24.9
	NdF_3	0.28	677.1	0.3	23.8

resolution. The multilayers move by linear translation at a speed of 1 step/800 ms. The complementary movement of the spectrometer keeps the setup on the Rowland circle.

Before each series of measurement, the setting of the pulse height analyser (PHA) has to be fixed. It avoids interfering signals as noise or higher diffraction orders, by the discrimination of the pulse amplitude. There are three different possibilities for the setting:

- differential mode: the lower and upper thresholds of the detection window have to be adjusted by hand;
- automatic differential mode: the detection window is automatically adjusted to the FWHM of the peak; and
- integral mode: every pulse passing above the lower threshold is counted provided that it remains below the saturation limit.

Comparison of the acquired spectra (Figure 3) shows that the differential mode is not suitable for the analysis of low-intensity lines as its discrimination window is too narrow. The automatic differential and integral modes can both be used as they give comparable P/B values.

In order to limit the influence of noise and higher diffraction orders, and in accordance with the recommendations in Reference 17 for boron analysis, the automatic differential mode was chosen for further measurements, (see also Figure 3).

Detection sensitivity and spectral resolution of analysing multilayers depend on the diffraction angle and better results are achieved when the characteristic X-ray's energy is located near the centre of the crystal's analysing domain. As a result, measurements should be carried out on the Ni/C multilayer for analysis of C and on the W/Si multilayer for N, O and F.

3.2 | Analysis

For easier identification of the different emission lines, higher diffraction orders on the measured spectrum and the peak shifts between their actual positions and the ones that are simulated with PENELOPE, it may be helpful to superpose the MC simulated spectrum with the measured one as shown in Figure 4. Here, the simulated spectra only account for background caused by Bremsstrahlung, MC simulations do not consider the valence band's DOS width contribution to the emission. Moreover, the background contribution of the spectrometer with its multilayers is not considered. This can explain the width difference between the simulated and the measured spectra shown in Figure 4.

The fitting process is the same for each sample: after the Kα emission line of the light element has been identified, the peak is fitted by Equation (3) to obtain information on the peak centre position, its FWHM and the shift that can be observed between the simulated peak and the measured one. The data tables (see Reference 15) used for the simulations do not take into account the chemical state of the emitting atom responsible for peak position changes.

To determine the best background description, the peak is cut depending on counting statistics between 1% and 10% of its intensity and the continuum is fitted by a third degree polynomial, an exponential and a linear function. Integration of the peak and the background intensities allows the determination of net intensity and P/B ratios for the three descriptions.

Figures 5 and 6 as well as Figures 7 and 8 show examples of the signal treatment for the samples Be and

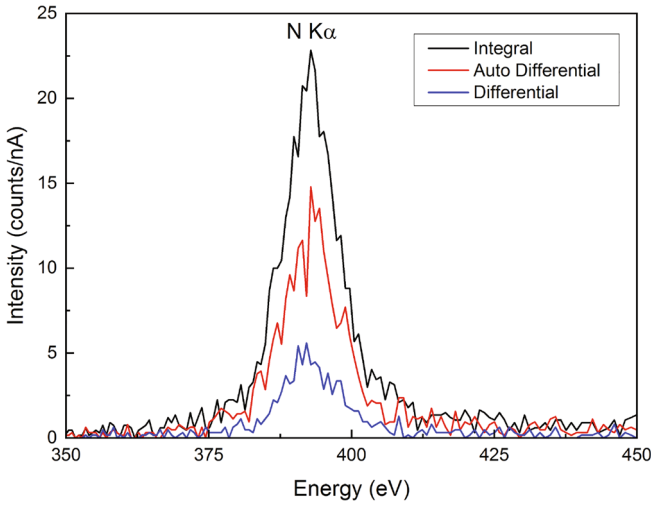

FIGURE 3 N Kα X-ray line emitted by a Si_3N_4 sample diffracted by the multilayer W/Si with three different pulse height analyser (PHA) settings. PHA setting in differential mode cuts most of the emission line and remaining intensity is only a few counts/nA, while automatic differential and integral mode lead to comparable P/B ratios. [Colour figure can be viewed at wileyonlinelibrary.com]

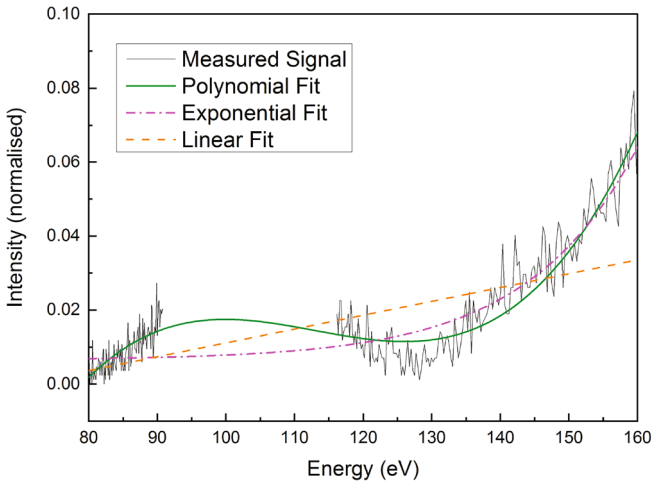

FIGURE 5 Polynomial, exponential and linear fits of the background of a characteristic X-ray spectrum acquired on Be. The coefficient of determination R^2 measures the goodness of the fit and is the best for the polynomial one: $R^2_{pol} = 0.974$, $R^2_{exp} = 0.94$, $R^2_{lin} = 0.473$. [Colour figure can be viewed at wileyonlinelibrary.com]

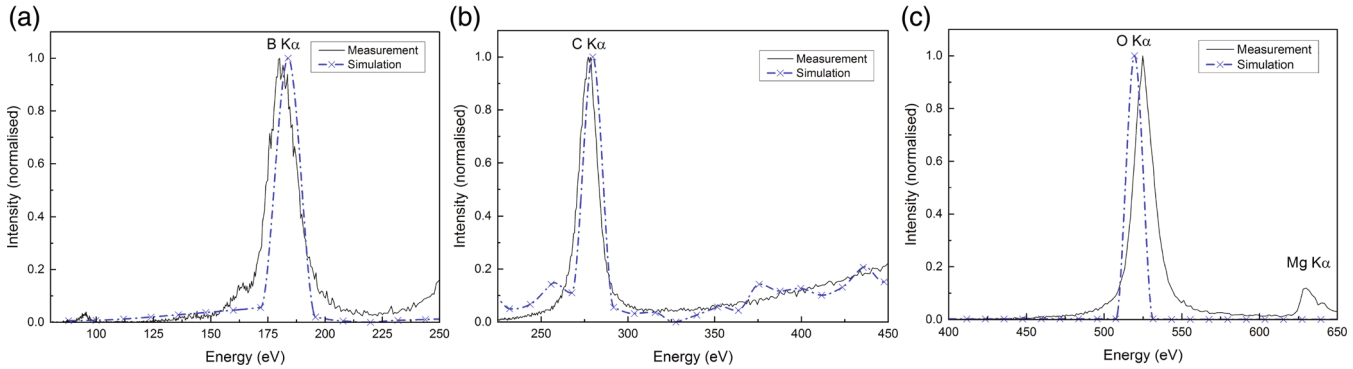

FIGURE 4 Superposition of measured and simulated spectra of the materials (a) $Mg_3B_7O_{13}Cl$, (b) SiC and (c) MgO. On (c) the second diffraction order of the Mg Kα line could be identified as noise as this peak does not exist in the simulation. [Colour figure can be viewed at wileyonlinelibrary.com]

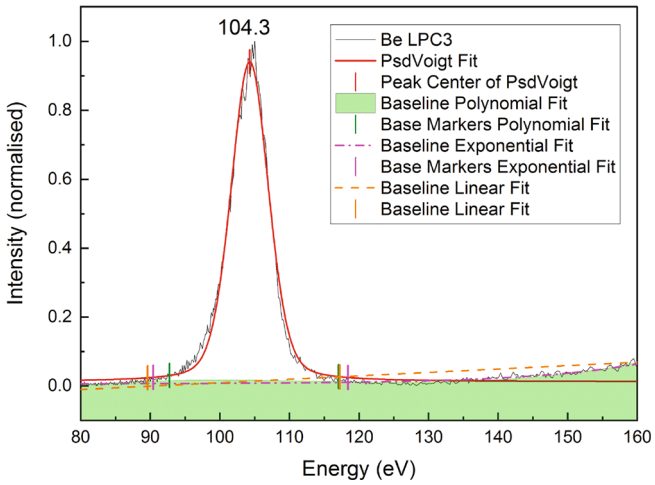

FIGURE 6 Pseudo-Voigt fit of the characteristic Be Kα peak with the three different background descriptions: The base markers define the integration area for net intensity and P/B ratios. [Colour figure can be viewed at wileyonlinelibrary.com]

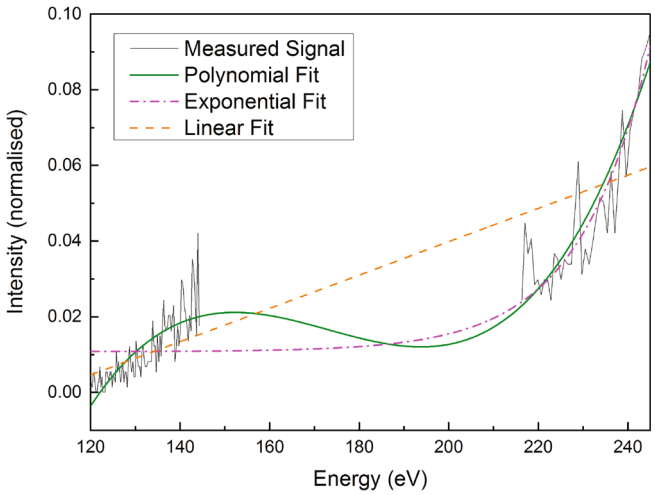

FIGURE 7 Polynomial, exponential and linear fits of the background of a characteristic X-ray spectrum acquired on $Mg_3B_7O_{13}Cl$. The coefficient of determination R^2 measures the goodness of the fit and is again the best for the polynomial one: $R^2_{pol} = 0.919$, $R^2_{exp} = 0.876$, $R^2_{lin} = 0.728$. [Colour figure can be viewed at wileyonlinelibrary.com]

$Mg_3B_7O_{13}Cl$. On Figures 5 and 7 the peak of the measured spectrum is cut and the background signal is fitted with the three different functions already mentioned. The three background fits are then transferred to the complete spectrum, with the Pseudo-Voigt fit of the characteristic emission (Figures 6 and 8). This allows, through background subtraction and peak integration, further signal treatment as described above.

Even if this data processing is time consuming, it allows an exact evaluation of the background description and ensures the absence of large errors in P/B calculations and therefore in quantitative EPMA.

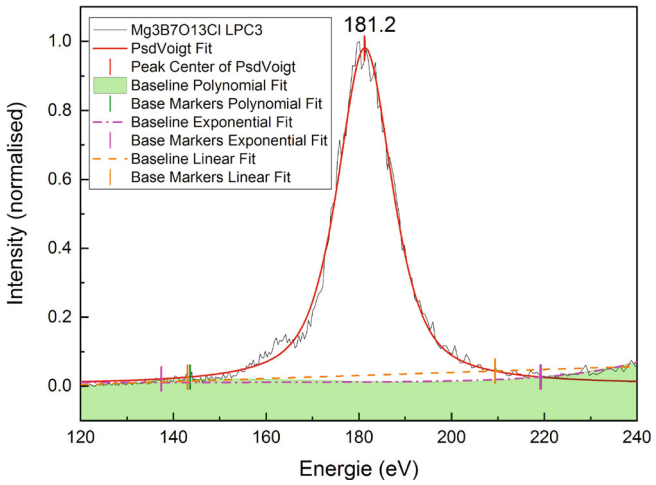

FIGURE 8 Pseudo-Voigt fit of the characteristic B Kα peak of a $Mg_3B_7O_{13}Cl$ sample with the three different background descriptions: The base markers define the integration area for net intensity and P/B ratios. [Colour figure can be viewed at wileyonlinelibrary.com]

4 | RESULTS AND DISCUSSION

The present section shows the results obtained by the data processing previously described for 25 samples that have been measured on the CAMECA SXFive FE TACTIS microanalyser and the multilayers listed in Table 1. Table 2 lists the results for this experimental setup and for simulations with MC PENELOPE. It gives information about the peak centre of the light element's characteristic emission line, the shift between the measured and the simulated position and its FWHM.

Table 3 lists the net intensity of the light element's Kα peak, the P/B ratios and the APFs for the three different background descriptions. If there was no pure sample of the light element, the APFs were calculated relative to the sample with the highest mass fraction. The results will not be discussed in detail but reviewed together for some measurement series.

The different peak shifts, caused by the differences in the emitting atom's chemical state depending on the material, have been pointed out. It could be observed that oxides undergo a more important shift (see Table 2 measurement series of B) in accordance to works carried out by Kasada et al.[18] The big shift of 4.2 eV of the Be Kα line to its simulated position is also due to oxidation. The simulation was made for pure Be metal but the sample oxidised. Fluorescence spectroscopy for chemical and valence band analysis carried out by Henke et al.[19] show that the characteristic Be Kα emission of BeO occurs at 105 eV. Exact knowledge of the different shifts is necessary to assess whether a separation of two neighbour lines emitted by different elements in the sample is possible or whether they will overlap. These kind of

TABLE 3 Net intensity of the emission line P/B ratios and area/peak factors (APFs) after subtraction of the background described by a polynomial, exponential and linear function

Material	I (eV)			P/B			APF		
	pol.	exp.	lin.	pol.	exp.	lin.	pol.	exp.	lin.
Be	6.62	6.87	6.74	16.97	28.63	17.74	1	1	1
B	17.00	17.23	17.32	24.29	34.46	42.24	1	1	1
LaB_6	15.88	15.96	15.88	14.70	15.35	14.05	0.93	0.93	0.92
$Mg_3B_7O_{13}Cl$	16.82	17.12	15.84	13.04	15.15	8.16	0.99	0.99	0.91
$CaB_2(SiO_4)_2$	14.69	14.92	11.30	5.05	5.14	2.89	0.86	0.87	0.65
Mo	21.77	24.78	22.75	1.48	1.96	1.53	1.28	1.44	0.74
C	18.68	18.82	18.17	26.31	30.85	17.81	1	1	1
SiC	15.36	14.56	12.63	13.02	7.79	4.68	0.82	0.77	0.70
TiC	14.25	14.33	14.39	13.57	14.25	15.31	0.76	0.76	0.79
Si_3N_4	10.22	10.80	10.84	5.91	6.97	6.45	1	1	1
GaN	10.79	10.93	10.33	3.11	3.21	2.51	1.06	1.01	0.95
TaN	6.54	6.67	5.16	1.34	1.39	1.03	0.64	0.62	0.48
SiO_2	18.05	18.96	19.14	9.25	14.36	14.61	1	1	1
$CaSiO_3$	18.49	18.71	18.49	11.24	11.41	10.51	1.02	0.99	0.97
MgO	17.58	18.03	18.01	11.57	14.78	14.18	0.97	0.95	0.94
$Ca_5(PO_4)_3F$	19.44	19.68	19.65	14.62	16.00	15.98	1.08	1.04	1.02
$Ca_3Fe_2(SiO_4)_3$	17.68	18.19	18.23	7.96	9.73	9.65	0.98	0.96	0.95
$ZrSiO_4$	18.00	18.55	18.34	7.09	8.21	7.37	1	0.98	0.96
$BaSO_4$	18.85	19.38	18.39	6.50	7.05	5.41	1.04	1.02	0.96
MnO	18.69	19.15	18.81	7.33	7.98	6.69	1.04	1.01	0.96
SnO_2	18.14	18.44	18.40	3.56	3.76	3.84	1	0.97	0.96
CeO_2	17.74	18.24	17.78	5.17	5.61	5.08	0.98	0.96	0.93
CeF_3	29.18	29.57	29.62	8.22	8.50	8.30	1	1	1
PrF_3	29.05	30.16	30.19	7.37	8.02	8.32	1	1.02	1.03
NdF_3	27.18	28.95	28.41	6.28	8.39	8.93	0.93	0.98	0.96

information are crucial for EPMA of samples containing light and heavy elements (e.g. B Kα line and Mo Mζ line or Li Kα line and Mg L and Al L lines).

For the analysis of borides together with Mo, one can expect a distance of ∼10 eV between the characteristic B Kα peak and the Mo ζ line. Therefore, to evaluate feasibility of X-ray separation, a closer look has to be taken on the FWHM values and the peak broadening caused by matrix effects more or less important for different material compositions. FWHM values may be insensitive to peak broadening and APFs can provide a better insight. For example, the FWHM values of the O measurement series vary less than 7% but the APF variations are at about 11%.

A closer look on P/B values reveals that for the polynomial description, in 23 of 25 cases, they are smaller than with an exponential or linear background description. Even if higher X-ray peak intensities facilitate EPMA quantification, one has to be careful to not underestimate the background but retain its best description. One has to be aware, that, once the energy and peak window are set for the background fit, the selection of the fitting functions is essentially mathematical. There is no physical reason to privilege the polynomial fit under the peak. Nevertheless, the background should be seen as a continuum and its description should be flexible enough to take into account the various physical phenomena that can occur close to the emission. That is why the third degree linear polynomial background fit was the best for all 25 analyses thus this description minimises quantification errors and should be used for the EPMA of light elements.

5 | CONCLUSION

The determination of optimised parameters for EPMA of light elements is a crucial step to minimise disruptive quantification errors. PHA should be set in an integral mode for emission lines with extremely low intensities in

the same order of magnitude as the background. Yet, overestimation of the peak's intensity is more likely to occur for acquisitions in integral mode and therefore, if possible, the PHA should be used in the automatic differential mode.

Accelerating voltages around 5 kV or even lower favour X-ray emission of light elements, but a compromise has to be found as working with low voltages forces the selection of L- and M-lines of heavier elements present in the sample. This generally results in poor quantification accuracy as the fundamental parameters are not precisely known and correction algorithms are not well working in this energy range.[20] As a consequence, an acceleration voltage between 9 and 12 kV may be the best choice. Simulation software as the program CASINO is an easy way to determine the best accelerating voltage setting in the microanalyser.

The comparison of polynomial, exponential, and linear background fits shows that the best background description for the emission spectrum of light elements is a third-degree polynomial function. P/B values are overestimated with exponential and linear fits.

When analysing light elements, one has to be aware that one will observe an emission band and not an emission line, which means that it is sensitive to the chemical state of the emitting atom. This will lead to peak shifts and peak shape changes for different material compositions. As a consequence, quantification should be carried out on the integral intensity of the emission band. When the response function of the spectrometer prevails, APFs can be used to save time.

ACKNOWLEDGEMENTS

Financial support for future works from the CEA cross-cutting basic research Programme RBNEW is gratefully acknowledged. The authors thank the reviewers for their thoughtful comments. The data that support the findings of this study are available from the corresponding author upon reasonable request.

DATA AVAILABILITY STATEMENT

The data that support the findings of this study are available from the corresponding author upon reasonable request.

ORCID

Pia Schweizer https://orcid.org/0000-0002-3735-9979

REFERENCES

[1] G. F. Bastin, H. J. M. Heijligers, *X-Ray Spectrom.* **1986**, *15*, 135.
[2] G. F. Bastin, H. J. M. Heijligers, *Scanning* **1990**, *12*, 225.
[3] C. Hombourger, P. Jonnard, J.-M. André, J.-P. Chauvineau, *X-Ray Spectrom.* **1999**, *28*, 163.
[4] V. Polkonikov, N. Chkhalo, R. Pleshkov, A. Giglia, N. Rividi, E. Brackx, K. Le Guen, I. Ismail, P. Jonnard, *Appl. Sci.* **2021**, *11*, 6385.
[5] M. J. Jercinovic, M. L. Williams, E. D. Lane, *Chem. Geol.* **2008**, *254*, 197.
[6] J. M. Allaz, M. L. Williams, M. J. Jercinovic, K. Goemann, J. Donovan, *Microsc. Microanal.* **2019**, *25*, 30.
[7] X. Llovet, A. Moy, P. T. Pinard, J. H. Fournelle, *Prog. Mater. Sci.* **2021**, *116*, 100673. https://doi.org/10.1016/j.pmatsci.2020.100673
[8] G. A. Rooke, *J. Res. Nat. Bureau Stand Sec A Phys. Chem.* **1970**, *74*, 273.
[9] J. L. Campbell, T. Papp, *At. Data Nucl. Data Tables* **2002**, *77*(1), 1.
[10] T. C. Huang, G. Lim, *X-Ray Spectrom.* **1986**, *15*, 245.
[11] R. Van Grieken, A. Markowicz, P. Van Espen, *Handbook of X-Ray Spectrometry*, (Ed: R. E. Van Grieken), 2nd ed., Marcel Dekker, Inc., New York **2002**, Ch. 4.
[12] R. Rinaldi, X. Llovet, *Microsc. Micoanal.* **2015**, *21*, 1053.
[13] X. Llovet, J. M. Fernandez-Varea, J. Sempau, F. Salvat, *Surf. Interface Anal.* **2005**, *37*, 1054.
[14] J. A. Bearden, *Rev. Mod. Phys.* **1967**, *39*, 78.
[15] X. Llovet, F. Salvat, *IOP Conf. Ser. Mater. Sci. Eng.* **2016**, *109*, 012009. https://doi.org/10.1088/1757-899X/109/1/012009
[16] D. Drouin, A. R. Couture, D. Joly, X. Tastet, V. Aimez, R. Gauvin, *Scanning* **2007**, *29*, 92.
[17] L. Cheng, C. Zhang, X. Li, R. Almeev, X. Yang, F. Holtz, *Microsc. Micoanal.* **2019**, *25*, 874.
[18] R. Kasada, Y. Ha, T. Higuchi, K. Sakamoto, *Sci. Rep.* **2016**, *6*, 25700.
[19] B. L. Henke, E. N. Smith, *J. Appl. Phys.* **1966**, *37*, 922.
[20] R. Wuhrer, K. Moran, *IOP Conf. Ser. Mater. Sci. Eng.* **2016**, *109*, 012019. https://doi.org/10.1088/1757-899X/109/1/012019

How to cite this article: P. Schweizer, E. Brackx, P. Jonnard, *X-Ray Spectrom* **2022**, *51*(4), 403. https://doi.org/10.1002/xrs.3290